*Journal Title Here*, 2022, 1–16
doi: DOI HERE
Advance Access Publication Date: Day Month Year
Paper

# Parametrization of biological assumptions to simulate growth of tree branching architectures

**Tristan Nauber[1,*] Ladislav Hodač[2] Jana Wäldchen[2,3] and Patrick Mäder[1,3,4]**

[1]Data-intensive Systems and Visualization Group, Technische Universitt Ilmenau, Ehrenbergstrae 29, 98693, Ilmenau, Germany, [2]Department Biogeochemical Integration, Max Planck Institute for Biogeochemistry, Hans-Knll-Str. 10, 07745, Jena, Germany, [3]German Centre for Integrative Biodiversity Research, iDiv (Halle-Jena-Leipzig), Puschstrae 4, 04103, Leipzig, Germany and [4]Faculty of Biological Sciences, Friedrich Schiller University Jena, Frstengraben 1, 07737, Jena, Germany

*Corresponding author. tristan.nauber@tu-ilmenau.de

FOR PUBLISHER ONLY Received on Date Month Year; revised on Date Month Year; accepted on Date Month Year

## Abstract

Modeling and simulating the growth of the branching architecture of tree species remains a challenge. With existing approaches, we can reconstruct or rebuild the branching architectures of real tree species, but the simulation of the growth process remains unresolved. First, we present a tree growth model to generate branching architectures that resemble real tree species. Second, we use a quantitative morphometric approach to infer the shape similarity of the generated simulations and real tree species. Within a functional-structural plant model (FSPM), we implement a set of biological parameters that affect the branching architecture of trees. By modifying the parameter values, we aim to generate basic shapes of spruce, pine, oak, and poplar. Tree shapes are compared using geometric morphometrics of landmarks that capture crown and stem outline shapes. Five biological parameters, i.e. xylem flow, shedding rate, proprioception, gravitysense, and lightsense, most influenced tree branching and their adjustments led to the generation of different spruce, pine, oak, and poplar shapes. The largest effect was attributed to gravity, as phenotypic responses to this effect resulted in different growth directions of gymnosperm and angiosperm branching architectures. Since we were able to obtain branching architectures that resemble real tree species by adjusting only a few biological parameters, our model is extendable to other tree species. Furthermore, the model will also allow the simulation of structural tree-environment interactions. Our simplifying approach to shape comparison between tree species, landmark geometric morphometrics, showed that even the crown-trunk outlines capture species differences based on their contrasting branching architectures.

**Key words:** Plant Physiology, Generative Modelling, Geometric Morphometrics, Functional-Structural Plant Models (FSPM)

## Introduction

For decades, researchers have tried to mathematically describe how trees grow, from simple modeling of branching patterns to approaches that include environmental conditions. Despite all these efforts, the question of how a typical spruce or oak shape develops, and what interplay of biological parameters plays an important role, remains unresolved: Can we parameterize tree growth to achieve the shapes of real tree species? And even if we can simulate trees, how is the shape of a tree defined? We seek to answer these questions for three reasons. (1) Tree branching architecture is often of taxonomic significance and can aid in accurate tree identification and taxonomic classification. (2) Tree branching architecture reflects ecological effects, including light interception, water and nutrient uptake, and interactions between trees and other organisms in the ecosystem. (3) Understanding the growth processes that lead to the actual branching architecture of trees can improve tree management practices, including planting and pruning.

An important part of the plant growth process is water transport. Assumptions such as the pipe model theory (Shinozaki et al., 1964) or Lockhart's equations (Lockhart, 1965) have been successfully used to approximate hydraulic architecture (Zimmermann, 1978), to study tree growth in terms of root and leaf elongation (Hsiao and Xu, 2000), or to study tracheid enlargement in pine (Cabon et al., 2020). Leaf gas exchange through photosynthesis initiates the water flow in the xylem, which is closely related to assimilation rates in the phloem. Approximations to simulate these effects at the whole tree level exist, but they reach their limits with large tree structures (Nikinmaa et al., 2014). Furthermore, the resulting change in osmotic potential in plant cells determines water demand and turgor, leading to phytohormone transport and various growth processes. The naming of these processes usually includes several underlying aspects. Concepts such as apical dominance or apical control are well known (Wilson, 2000; Kadereit et al., 2014; Hollender and Dardick, 2015), but a mathematical description of them is not trivial. The orientation of plant organs is a separate area of research. Initially, gravitropic orientation was mathematically defined as the gravitropic set-point angle (GSA) (Digby and Firn, 1995). By adding a light dependence it became the photogravitropic equilibrium (Galland et al., 2002). Further ideas added a dependence on proprioception, the perception of local curvature, leading to the $A_rC$ model (Bastien et al., 2013, 2015). This model has been successfully studied in woody species (Coutand et al., 2019). It is possible to simulate plant tropism by coupling hormone transport to local tissue deformation (Moulton et al., 2020). Such input-output systems are useful for a robust mathematical description (Meroz, 2021). Modern concepts include further aspects such as the sagging of branches under their own weight (Moulia et al., 2022). However, the internal mechanisms are not yet fully understood. The challenge is to map the different processes simultaneously, but our understanding of the underlying mechanisms and patterns is still incomplete (Muller-Landau et al., 2021; Piovesan and Biondi, 2021; Li et al., 2022).

The sum of individual processes over many years results in the final characteristic shape of a mature tree. Architectural approaches are usually applied to describe the branching structure of trees (Hallé et al., 1978; Barthélémy and Caraglio, 2007). We are aware of very few attempts to mathematically analyze the shape of real tree species, but they based on machine learning assumptions. For example, the use of artificial neural networks with a multilayer perceptron architecture to predict the characteristics of tree species growing in an open landscape (Bueno et al., 2022), or an analysis for visual realism of generated tree models using a convolutional neural network and automated similarity metrics (Polasek et al., 2021). Analysis of the overall shape of the tree crown can provide insight into branching patterns and architectural features. It is known that tree crown shape is a criterion for species identification and delimitation (Schmidt, 1980; Duchemin et al., 2018). However, it is unclear how the final characteristic shape of particular tree species is defined. In plant systematics, leaf and flower shape or bark texture are common features used to distinguish tree species (Liu et al., 2018). Shape analysis techniques, such as geometric morphometrics, can help quantify and compare the crown shapes of different tree species, providing a means to study the relationship between tree architecture and overall crown shape. Geometric morphometrics has been widely used to analyze the shapes of tree leaves (Jensen et al., 2002; Nicotra et al., 2011; Du et al., 2022), flowers, and even pollen (Caiza Guamba et al., 2021), but its application to comparing whole tree shapes is limited.

The origin of tree modeling began with the formulation of growth as a simplified rule-based process with recursively connected branches (Honda, 1971). This approach has been developed in various ways (Fisher and Honda, 1977; Honda et al., 1982; de Reffye et al., 1988; Weber and Penn, 1995), and Prusinkiewicz and Lindenmayer (Lindenmayer and Prusinkiewicz, 1990) published a list of algorithms that can be used to model a wide variety of trees and their properties. Subsequent work has considered interactions with environmental factors as key factors in the development of plants and plant ecosystems (Prusinkiewicz et al., 1994; Měch and Prusinkiewicz, 1996). These include approaches that approximate the environment as particle systems (Reeves and Blau, 1985), by ray-casting (Arvo and Kirk, 1988), or as voxels (Greene, 1989). The method of self-organizing tree modeling (SOTM) (Palubicki et al., 2009) improved this approach and considered the concept of Sachs, where a self-organizing character of bud and branch growth was considered (Sachs, 2004). SOTM presents possible assumptions for simulating tree growth based on different environmental approximation and resource allocation strategies (Runions et al., 2007; Borchert and Honda, 1984). Such models, which describe the complex interactions between plant architecture and physical and biological processes, are known as functional-structural plant models (FSPMs) (Godin and Sinoquet, 2005). In recent decades, FSPMs have been used to model various aspects of plant biology and plant community ecology (Vos et al., 2010). They are capable of handling a wide range of growth and development processes, from microscopic cell division to macroscopic modeling of entire plant communities (Makowski et al., 2019; Louarn and Song, 2020; Crimaldi et al., 2021).

While many previous approaches produced visually appealing results, they did not guarantee a reproducible and biologically meaningful arrangement of individual tree organs and branches. We aim to create a computationally robust FSPM at the level of tree organs to reproducibly simulate the growth of real tree species. We hypothesize that the branching architecture of real tree species can be described by a limited number of parametrizable biological factors and aim to answer the following questions: (1) Can parameterized biological processes help simulate the growth of real tree branching architecture? (2) Can geometric morphometrics distinguish tree shapes based on their reduced outline representations?

(3) Which of the 14 selected biological parameters have the strongest influence on tree shape growth? To address these questions, we built a simple FSPM inspired by biological processes. The evaluation of the model performance includes a geometric morphometric analysis between the self-generated tree models with real tree species inferred from photographs and illustrations.

## Materials and Methods

### Model description

We use a functional-structural plant model (FSPM), which consists of an iterative interaction between the biotic and abiotic environment. The biotic environment is reduced to a single tree and operates at the plant and organ level (Fig. 1a). The root system is interpreted as a simple interface that determines water uptake. The leaves are considered as terminal components that produce sucrose through photosynthesis. They use the incoming light from the environment and transpire water. The resulting water loss causes a decline in water potential, inducing the internal flow mechanism. The tree model uses a graph of interacting nodes as a basic concept. A node represents a location in the tree structure. It contains both spatial and resource information. The connection between two nodes defines an internode. A list of nodes and internodes represents a branch, and the connections between multiple branches create the graph that represents the tree structure. Young shoots are branches consisting of light-sensitive nodes. Buds produce new nodes and internodes. They represent apical or lateral meristems and are interpreted as terminal nodes. The activity of the meristems can be in different states. In the case of an inactive bud, no further nodes are produced. This state is called dormancy. When growth resumes, budding occurs. The activity of the meristems is controlled both by internal phytohormones and by changes in the abiotic environment. These internal processes of a single tree and changes in the abiotic environment are simulated by a growth cycle (GC) and an environmental update (EU). An overview of their working principles is given below, while the details of their subfunctions are explained in the following parts of this section.

#### Growth-cycle (GC)

To simplify the growth description of perennial woody plants, we use a growth cycle (GC) (Fig. 1b), which represents an annual cycle. We assume that there is an internal flow of water and sucrose, including phytohormones, that causes different growth conditions at the plant level. A complete GC begins with an input of environmental conditions. This information is used to control which meristems enter or exit dormancy (bud fate), to control resource allocation (apical control), and to determine the resulting growth activities (growth). Both the orientation by light and the influence of gravity are calculated (tropism). The amount of sucrose produced is then determined and the available resources are processed. This determines possible growth conditions for the next GC. The final step is to remove unwanted or damaged organs (shedding).

#### Environmental update (EU)

The interaction between the tree and its environment is computed iteratively in the environmental update process (EU; Fig. 1b). A free-standing tree has a wide distribution of light across the hemisphere. Combined with factors such as regular cloud cover, this results in a very diffuse light. Branches and leaves cast shadows according to their size. As the distance increases, the shadow becomes fainter. This fading effect creates a soft shadow effect. We use a voxel system to estimate such light distribution in space (Greene, 1989), where each voxel (x, y, z) represents a shadow value $s_{val}$ (Palubicki et al., 2009). The voxel size ($v_{size}$) determines the level of detail, while the voxel depth ($v_d$) controls how wide the shadow is cast on the Z-axis ($-v_d \leq \Delta z \leq 0$). The lateral shadow width ($s_w$) is controlled with $w_s(z) = \lfloor |z|^{s_w} \rfloor$. We assume that the shadow is evenly distributed along the X and Y axes ($-w_s(z) \leq \Delta x, \Delta y \leq w_s(z)$). The shadow cast ($s_t$) per node is determined by the throw intensity ($0 \leq a \leq 1$), the fading of shadowing per voxel ($b > 1$) and cast width:

$$s_t(\Delta x, \Delta y, \Delta z) = a \cdot b^{-(0.1 \cdot (|\Delta x| + |\Delta y| + |\Delta z|) \cdot V_{size})} \quad (1)$$

The shadow value $s_{val}$ of a voxel is calculated as the sum of all shadow casts. It determines the resulting light value $l_{val}$:

$$l_{val} = max(1 - s_{val}(x, y, z), 0) \quad (2)$$

The incoming light ($\vec{I}$) for a node is calculated by considering all light values of neighboring voxels.

#### Basic pattern

We define the basic pattern of a tree as the node topology of a stem and its lateral branches. Based on the idea that each leaf has an axillary bud, phyllotaxis is used to determine the possible arrangement of lateral buds (Notes S1). We define the number of leaves per node $N$, and the rotation around the stem a divergence angle $\varphi$. The branching angle is defined by the parameter $\theta$. The number of nodes added during budding is defined by the parameter $NN$ and the distance between two nodes by the internode length parameter $\rho$.

#### Bud fate

Buds do not always start growing immediately (Notes S2), they go through a period of dormancy depending on phytohormones and environmental conditions (Wilson, 2000; Hollender and Dardick, 2015). To define the order of outgrowth buds, we use the term acrotony as topological arrangement ($s_{ac}$) and the term epitony as spatial orientation ($s_{ep}$), as described by Barthélémy (Barthélémy and Caraglio, 2007). Their sum, in dependency of their influence $f_{ac}$, $f_{ep} \in [0, 1]$, is used to define a sort-value ($s$) in Eqn. 3.

$$s = (s_{ac} \cdot f_{ac}) + (s_{ep} \cdot f_{ep}) \quad (3)$$

$s$ in combination with the idea of the priority model (Palubicki et al., 2009) determines which lateral buds break dormancy. All buds ($m$) on a branch are sorted in a list by the minimum of the given sort-value $s$. The resulting index ($i = 1, 2, ..., m$) of each bud represents its priority and is used in a linear weight function $w(i) = \frac{i}{m}$. As soon as $w(i)$ exceeds the budding rate threshold ($BR$), the dormancy breaks and budding is activated.

The topological alignment depends only on the internal node structure of the current branch. For this purpose, we use the acrotony parameter ($ac \in [0, 1]$), in dependency with the total number of nodes in the branch ($NN_b$) and the topological position of the

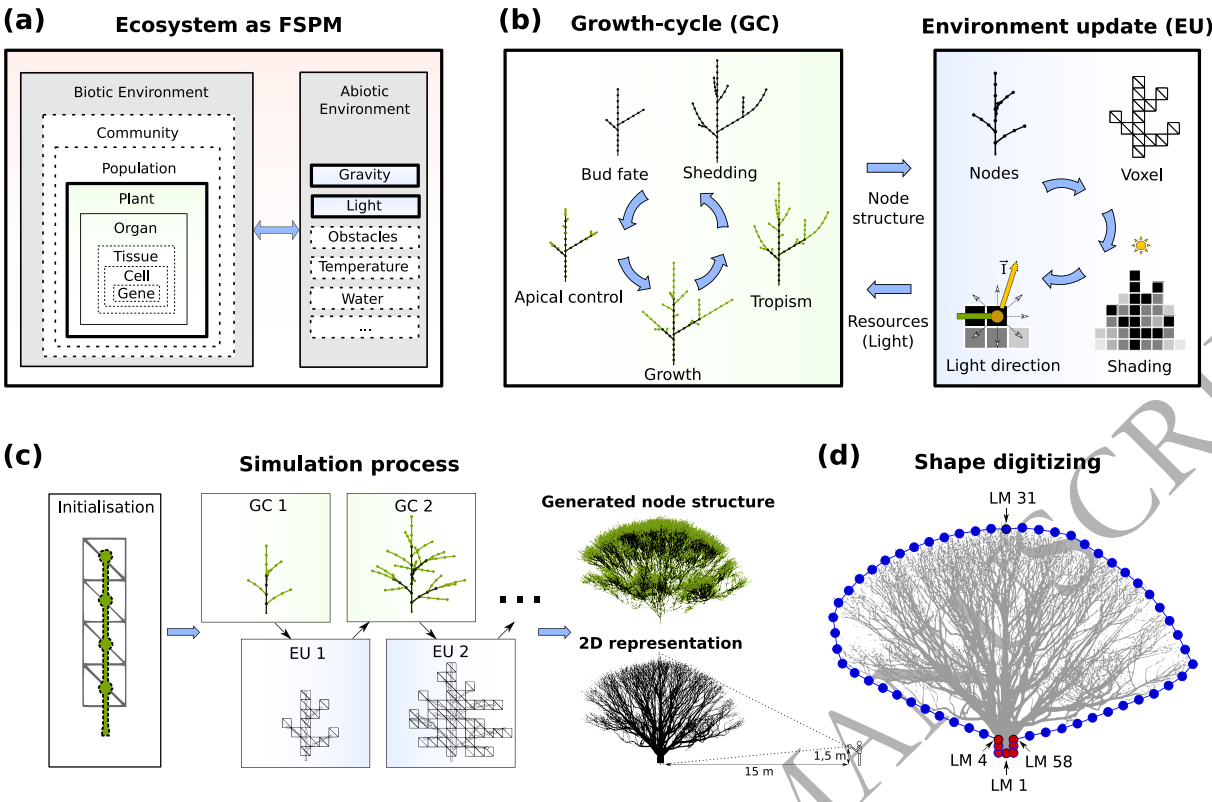


Fig. 1: Model Overview: a) ecosystem as the approximate interplay between the biotic and abiotic environment, b) growth cycle (GC) as a repeated internal calculation of the tree structure and environmental update (EU) as its continuous environmental impact, c) simulation process from structure initialisation to the final 2D representation of the tree, and d) tree shape delimitation using stem landmarks (red) and crown landmarks (blue).

current node ($tp$), in Eqn. 4.

$$s_{ac} = \frac{|(NN_b \cdot ac) - tp|}{NN_b} \tag{4}$$

The spatial orientation, on the other hand, depends on the direction of gravity. This is achieved by using the scalar product ($\circ$) of the normalized vectors for node orientation ($\vec{n}$) and gravity direction ($\vec{g}$), which represents the cosine of the angle between these vectors. $s_{ep}$ is finally controlled by the epitony parameter ($ep \in [0, 1]$) in Eqn. 5.

$$s_{ep} = |\frac{(\vec{n} \circ \vec{g}) + 1}{2} - ep| \tag{5}$$

### Apical control

The term apical control summarizes a complex allocation of resources and interplay of phytohormones. Within the branching structure, apical control influences several aspects of growth. A substantial part of this allocation is based on the distribution of water in the xylem and sugar in the phloem. We use the extended Borchert-Honda (BH) model (Borchert and Honda, 1984; Palubicki et al., 2009) to approximate a unidirectional flow of water and nutrients from root to leaf that induces shoot elongation (Eqn. 6). Instead of using the amount of light, we use the approximated negative water potential ($\Psi$). For the elongation process, we assume that $\Psi$ depends mainly on the osmotic potential, which is based on the amount of sugar per bud from the previous iteration ($\Psi = Q_{t-1}$). The xylem flow parameter $\lambda$ controls how $\Psi$ at a branching point distributes the water ($H2O$) between the continuing main axis ($\Psi_m$, $H2O_m$) and the lateral branch ($\Psi_l$, $H2O_l$).

$$H2O_m = H2O\frac{\lambda\Psi_m}{\lambda\Psi_m + (1-\lambda)\Psi_l} \quad and$$

$$H2O_l = H2O\frac{(1-\lambda)\Psi_l}{\lambda\Psi_m + (1-\lambda)\Psi_l} \tag{6}$$

The BH model is later used in a second pass to approximate the photosynthesis calculation and the resulting sugar allocation ($Q$) per bud in the shedding section below.

### Growth

To simulate growth, we use the concept of reiteration, where the organism duplicates its own elementary architecture (Barthélémy and Caraglio, 2007). When a bud breaks its dormancy, it produces new phytomers. Therefore, we use a growth activity $ga$ initialized with the amount of sugar available to the bud ($ga = NN \cdot Q_{t-1}$). This value is used to add iterative nodes to the branch. Eqn 7 shows, how the parameter $\tau$ approximates the influence of the apical dominance. Each time a node is added, the growth activity for the apical bud $ga_a$ and the newly created lateral buds $ga_l$, is updated by $\tau$. These buds repeat this process,

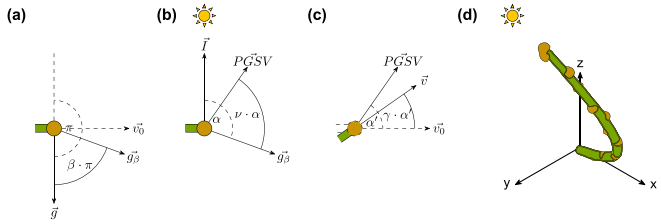


Fig. 2: Calculation of Tropism by the gravitropic set-point vector $\vec{g_\beta}$ (a), photogravitropic set-point vector $P\vec{G}SV$ (b) and the resulting direction vector $\vec{v}$ (c). d) shows an example off the curvature of a young shoot with 12 nodes in 3D-space.

reducing the growth activity until it reaches zero.

$$ga_a = ga \cdot \frac{(1+\tau)}{N+1} \qquad and \qquad ga_l = \frac{ga - ga_a}{N} \tag{7}$$

We assume that elongation occurs only in the internodes of a young shoot. The amount of elongation ($length$) is determined by an equal share of the available amount of water $H2O$ and a defined internode length $\rho$ over number of nodes $NN_y$ of the young shoot (Eqn. 8).

$$length = \frac{\rho \cdot H2O}{NN_y} \tag{8}$$

For cambium activity we use the idea of the pipe model (Shinozaki et al., 1964; Palubicki et al., 2009) and assume that each phytomer needs a vascular connection for its base. The width of an internode ($d'$) results from the sum of the cross sections for the number of added phytomers $NN_p$ on the topological structure. The previous width $d$ and the initial width for a phytomer $d_0$ determine the resulting width in Eqn. 9.

$$d' = \sqrt[3]{d^3 + (NN_p \cdot d_0^3)} \tag{9}$$

**Tropism**

The initial orientation $\vec{v_0}$ of an annual shoot is determined by the phyllotaxis-based pattern of its original axial bud. To simulate tropism, we compute the curvatures of a young shoot (Fig. 2d). The incoming light $\vec{I}$ and gravitational direction ($\vec{g}$), as normalized orientation vectors, are the basis for this calculation. We parameterize the underlying biological process graviceptive sensitivity as gravitysense($\beta$), proprioceptive sensitivity as proprioception ($\gamma$), and phototropic sensitivity as lightsense ($\nu$). The resulting direction $\vec{v}$ is calculated as the rotation between the resulting vectors. In Fig. 2a we show how $\beta$ controls the gravitropic set-point vector $\vec{g_\beta}$. With $\nu$ we calculate the effect of the light direction $\vec{I}$. The resulting photogravitropic set-point vector $P\vec{G}SV$ approximates the influence of light and gravity (Fig. 2b). Finally, we use $\gamma$ to control the reorientation of a node (Fig. 2c,d).

**Shedding**

Since that there is at least one leaf per bud, the sucrose produced by photosynthesis represents the sugar ($Q$) available to the bud. We again use the BH model (Eqn. 6) to approximate the distribution of resources. In this second pass, we assume that the water potential is mainly based on leaf transpiration rates induced by incident light from the light distribution model ($\Psi = l_{val}$). We have added the assumption that the distributed water $H20$ reflects the potential for sugar production, but even if more water is available, there is not enough energy to produce more sugar. The amount of sugar is calculated as the minimum between incoming light and available water.

$$Q = min(l_{val}, H20) \tag{10}$$

For each branch, we determine the amount of sugar produced per node. To do this, we use a basipetal pass, from leaves to root, to obtain the accumulated sugar values $Q_a$ for each branch. A branch is removed if the amount of sugar produced compared to the number of all nodes the branch carries ($NN_a$) is less than the shedding rate parameter $\kappa$.

$$\frac{Q_a \cdot NN}{NN_a} < \kappa \tag{11}$$

The number of nodes per budding $NN$ is necessary to make $Q_a$ comparable to $NN_a$. All defined parameters (Table 1) are used to simulate the growth of the tree.

**Table 1.** Model parameters for exogenous and endogenous growth.

| Symbol | Name | Reference of original idea |
|---|---|---|
| $N$ | Leaf number | ($m$) (Fisher and Honda, 1977) |
| $NN$ | Node number | ($N_s$) (Borchert and Honda, 1984) |
| $\varphi$ | Divergence angle | ($\alpha$) (Honda, 1971) |
| $\theta$ | Branching angle | ($\theta$) (Honda, 1971) |
| $\rho$ | Internode length | ($R$) (Honda, 1971) |
| $\gamma$ | Proprioception | ($\gamma$) (Bastien et al., 2013) |
| $\nu$ | Lightsense | (Greene, 1989) |
| $\beta$ | Gravitysense | ($\beta$)(Honda et al., 1982) |
| $\kappa$ | Shedding rate | ($P_{min}$)(Takenaka, 1994) |
| $\lambda$ | Xylem flow | ($\lambda$)(Palubicki et al., 2009) |
| $\tau$ | Apical dominance | ($f$)(Honda et al., 1981) |
| $BR$ | Budding rate | (Palubicki et al., 2009) |
| $ac$ | Acrotony | (Barthélémy and Caraglio, 2007) |
| $ep$ | Epitony | (Barthélémy and Caraglio, 2007) |

## Sampling of tree shapes for geometric morphometric evaluation

In total, we analyzed 1000 tree shapes from three different sources: (1) self-generated tree growth simulations (ST), (2) photographs of real tree species (PT), (3) illustrations of real tree species (IT). Our selection of angiosperm and gymnosperm species common to Central Europe are representative of a variety of different forms. ST targeted four different tree forms: spruce (*Picea*), pine (*Pinus*), poplar (*Populus*), and oak (*Quercus*). PT and IT include the corresponding real tree species: spruce (*Picea abies*), pine (*Pinus sylvestris*), poplar (*Populus nigra 'italica'*), and oak (*Quercus*

*robur*). To expand the geometric morphometric dataset of real tree shapes, we added four additional species to both PT and IT, maple (*Acer pseudoplatanus*), beech (*Fagus sylvatica*), fir (*Abies alba*), and larch (*Larix decidua*).

### Ground truth data - real tree photographs (PT) and illustrations (IT)

For the geometric morphometric comparison of the shapes of real tree species, we prepared a dataset consisting of 25 PT and 10 IT for eight tree species. PT were obtained from the Global Biodiversity Information Facility (GBIF, 2022) image database and the Flora Incognita project (Boho et al., 2020). IT were obtained from publicly available tree atlases. The 280 images from PT and IT were used as ground truth for the evaluation of ST. Suitable images of real tree species met the following criteria: solitary tree and as few background objects as possible (Fig. S2).

### Self-generated tree growth simulations (ST)

We implemented the growth simulation in C++ and visualized the branching pattern of the trees using Unreal Engine 5. We generated 720 3D-tree models with corresponding 2D representations (Fig. 1c) while varying the parameters (Notes S3). We used a perspective projection to convert the 3D tree models into 2D images. The virtual camera was set to a distance of 15m (Y-axis), a height of 1.5m (Z-axis) and a field of view of 60°. Each image shows the branching structure of the tree in black and the background in white.

## Evaluation of similarity between simulated and real trees

The statistical evaluation of the simulated trees was done in three steps:

1. Approximation of crown and trunk shape with 2D-outlines
2. Capturing the tree outlines with trunk and crown landmarks
3. Quantitative comparison of the tree shapes of different species and tree simulations with geometric morphometrics

### Approximation of crown and trunk shape with 2D-outlines

We approximated the tree crown and trunk shapes with their 2D silhouettes/outlines. The acquisition of the tree outline shape was either fully automated (for the generated tree simulations) or semi-automated (for the images and illustrations of real tree species). Finally, each tree outline was captured by a set of 60 x/y coordinates (landmarks), and we illustrate the landmark digitization procedure using an image of an oak tree (Fig. 3; Fig. S3).

For the fully automated landmarking of the generated tree simulations, the trunk outline was automatically captured by seven automatically placed landmark points. The crown outline was automatically captured by an algorithm that placed an x/y point at each branch tip, and based on these points, the Quickhull algorithm (Barber et al., 1996) generated a convex hull for the left and right halves of the crown outline. In each case, the mid-axis was defined by landmark LM 1 (trunk base) and landmark LM 31 (highest branch tip/highest crown extremity). On the computed convex hull, an algorithm placed 26 equidistant landmarks at each half of the crown outline.

The procedure for the semi-automatic landmarking of the real tree species images and illustrations was similar to that described above for the generated trees. The only difference was that we manually placed the seven trunk landmarks and also manually selected the initial branch tip points to optimally capture most of the crown outline extremities. The computation of the convex hull on the crown outline was done with the same Quickhull algorithm as described above, and the placement of the mid-axis and the final 26 equidistant landmarks on both sides of the crown was also done as described above. The two points in the middle of the trunk have also been auto-adjusted to be exactly halfway between the base of the trunk and the base of the crown. The trunk points LM 1, 3, 5, 6, 8 were not automatically adjusted.

The manual steps of landmark digitization as well as the visualization of the landmark configuration were done in the TpsDig software (Rohlf, 2015).

### Capturing the tree outlines with trunk and crown landmarks

The outline shape of each tree was captured by seven trunk landmarks and 53 crown landmarks; Fig. 1d). The seven landmarks (LM 1-4 and LM 58-60) described the shape of the trunk, i.e. from the base of the bilateral symmetry axis (LM 1) to the position of the first lateral branches (LM 4 and LM 58). Another 53 landmarks captured the shape of the crown outline, while the landmark LM 31 was always placed on central axis at the top of the crown of each tree. We applied landmark data standardization via Procrustes superimposition to align all outline shapes and compute the reference or consensus configuration (mean shape). The Procrustes superimposition (Rohlf and Slice, 1990) achieves uniform position, orientation, and scaling of all landmark configurations under comparison, and separates asymmetric and symmetric components of shape variation (the symmetry axis is given by landmarks 1 and 31). The crown landmarks placed along a curve (i.e., 'semilandmarks') were allowed to slide along the outline curve during the Procrustes superimposition (Bookstein, 1997). This step was done in the TpsRelw software (Rohlf, 2015).

### Quantitative comparison of the tree shapes of different species and tree simulations with geometric morphometrics

The aligned and symmetrized Procrustes coordinates were used to extract shape variables for subsequent use in multivariate statistics (Zelditch et al., 2004). The extraction of shape variables was performed by principal components analysis (PCA) of the aligned Procrustes coordinates, also known as relative warp analysis (RWA). The scores of tree shapes on the principal components (relative warps) were used to infer similarity of tree shapes. To infer dissimilarity of predefined groups of tree shapes, we used either pairwise discriminant analysis (DA) or multigroup discriminant analysis, also known as canonical variates analysis (CVA) (Klingenberg, 2011; Du et al., 2022). All morphometric analyses were performed using MorphoJ software (Klingenberg, 2011). Graphical outputs of multivariate ordination techniques (2D and 3D scatterplots) were visualized using Tikz. Changes in tree shape or mean shapes of groups were illustrated by wireframe plots exported from MorphoJ software.

## Results

### Simulated tree growth inspired by biological processes

#### Behavior of tree shape simulation

The default tree in Fig. 4 visualizes a basic assumption for realistic tree growth conditions. It is based on a spiral pattern, equal water

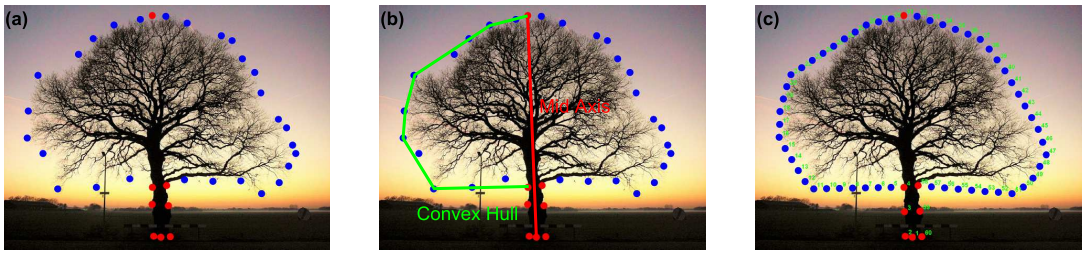


Fig. 3: Tree shape extraction from image data: (a) manual placement of seven landmarks on the trunk outline and manual placement of an arbitrary number of landmarks on the crown outline, (b) automatic computation of the convex hull that captures the crown outline and the mid-axis connecting the highest and lowest points of the tree shape and defining the bilateral symmetry axis, (c) automatic computation of the final set of 53 equidistant landmarks along the crown outline using the convex hull as a guide.

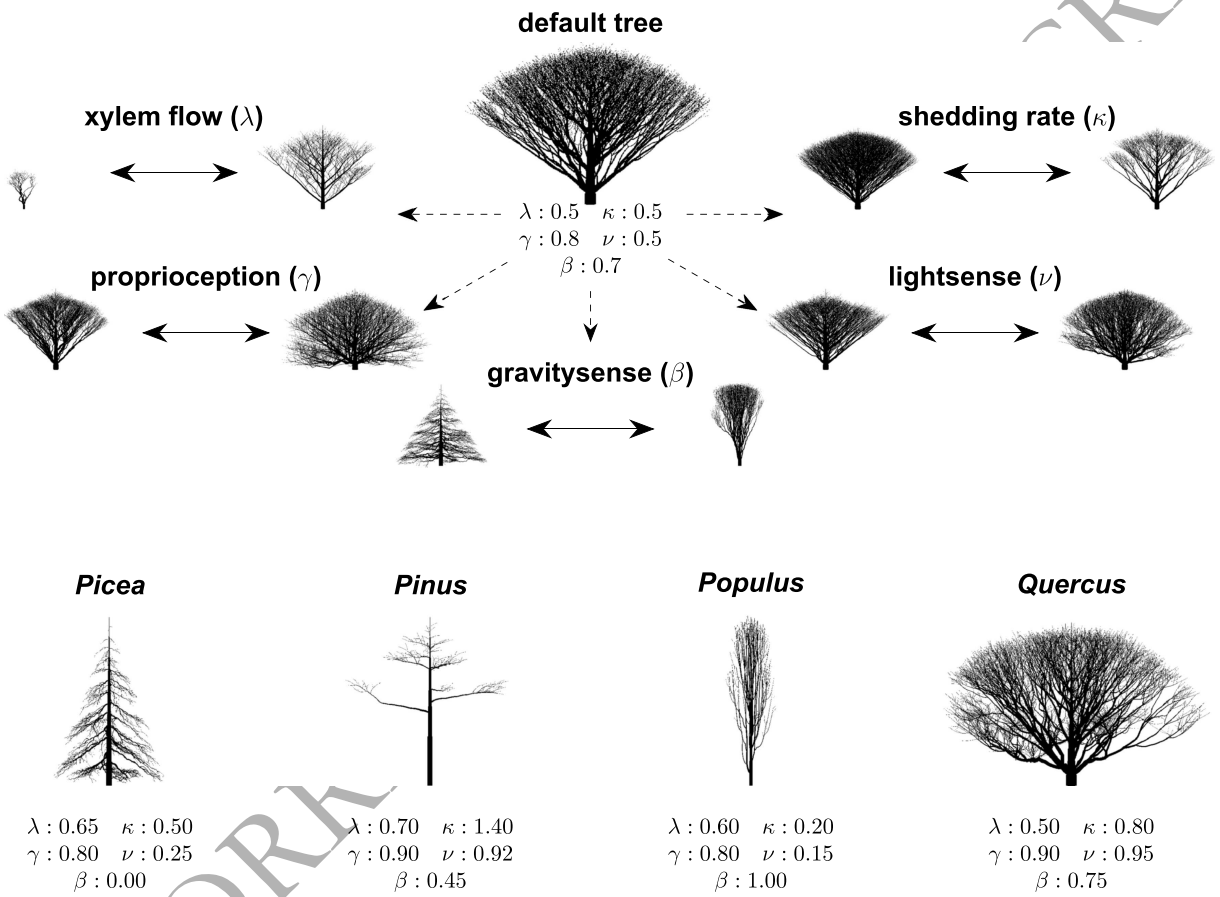


Fig. 4: Tree simulations from a common default parameter set ($N = 1$, $\phi = 137.5°$, $\theta = 60°$,$NN = 10$, $\rho = 5$). The default tree illustrates the variation of a single parameter change between minimum and maximum values. The lower part illustrates generated tree simulations of spruce (*Picea*), pine (*Pinus*), poplar (*Populus*), and oak (*Quercus*) resulting from four different parameter set adjustments.

distribution throughout the tree, medium shedding of branches and a tendency to bend vertically upward. The basic pattern for each branch growth is defined by its phyllotaxis ($N$, $\phi$, $\theta$) and branching settings ($\rho$,$NN$). The branching settings determine how the space around the branch is filled, and remain constant for all branches as long as no additional influences occur.

Lateral bud outgrowth is controlled by $\tau$. At low values, lateral buds can grown out without a phase of dormancy. This results in a slower increase in crown width over time. Bud fate ($BR$, $ac$, $ep$) only affects young shoots. The effect is similar to the basic pattern. The apical meristems die when basiotony occurs, and the resulting tree simulation loses its characteristic tree-like shape.

The self-regulation of the tree's branching architecture is controlled by $\kappa$ and $\lambda$. A high $\kappa$ removes even slightly shaded branches and thins the tree crown. This affects the lower part of the crown. $\lambda$ provides a parameter to control the distribution of water between apical and lateral branches. If $\lambda \leq 0.5$, the lateral branches will grow as fast as or faster than the apical leader. This results in a

decurrent tree shape with a broad crown (i.e., oak-like rounded or spreading crown, with multiple scaffold branches). For $\lambda > 0.5$ the apical leader will grow faster than the lateral branches below it. This results in an excurrent tree shape with a single central stem and a conical crown (i.e., spruce-like cone-shaped crown with a central leader).

$\gamma$ controls how strongly the original orientation of a branch is maintained. If $\gamma = 1$, then there is no response to light and gravity. It determines how fast the photogravitropic set-point vector $P\vec{G}SV$ is reached. $\nu$ controls the response to light. If $\nu = 0$ no light will be received. $\beta$ determines the preferred direction of growth, as long as $\gamma < 1$ and $\nu < 1$.

**Simulations of real tree forms: spruce, pine, poplar, oak**

Adjusting the parameters according to biological assumptions changes the resulting visualization for the tree simulation (Fig. 4). The simulated growth of spruce (*Picea*) is based on strong suppression of lateral growth ($\lambda \geq 0.65$), low sensitivity to light ($\nu < 0.3$) and a tendency to bend in the direction of gravity ($\gamma < 0.4$). The growth of pine (*Pinus*) is also based on a strong suppression of lateral buds, but with a high sensitivity to light ($\nu > 0.9$) and a high rate of shedding ($\kappa > 1.2$). In contrast, the growth simulation of poplar (*Populus*) is based on a strong orientation against gravity ($\gamma > 0.9$) and a low sensitivity to light. Finally, the growth simulation of oak (*Quercus*) is determined by an equal water content ($\lambda = 0.5$) and a plagiotropic tendency of the branches.

## Geometric-morphometric evaluation of real tree shapes

**Analysis of eight tree species derived from real tree photographs**

Ordination of the eight real tree species shapes along the first two principal components allowed visual interpretation of major morphological trends within the tree morphospace (Fig. 5a,b). The largest variation (69%) concerns the general shape change from broad, oak-like wide crowns to conical, poplar-like crowns (Fig. 5a). The second most important morphological trend (20%) described the shape change from long to short stems below the first lateral branches (Fig. 5a). Other morphological trends described rather minor shape changes in the shape of the crown base (6%) and in the shape of the upper part of the crown (2%; Fig. 5b). Discriminant analysis of the two major tree groups (gymnosperms vs. angiosperms; Fig. 5c) revealed a significant difference between the mean gymnosperm and mean angiosperm tree shape, with differences affecting both the base and the top of the crown (Fig. 5d). The gymnosperms-angiosperms separation was tested by cross-validation with a slightly higher correct classification rate for gymnosperms (87%) than for angiosperms (86%).

The average excurrent tree shape within the gymnosperms and the average decurrent tree shape within the angiosperms are illustrated in Fig. 5c. Exceptions are *Pinus* and *Populus*. For *Pinus*, the longer stem in relation to its round crown represents the average tree shape. In the case of *Populus*, the crown has a small width resulting in a columnar shape. *Pinus* and *Populus* represented two extremes within the tree species morphospace. *Pinus* shapes formed a grouping in the negative range of PC2 and also shows an increased dispersion of tree shapes. *Populus* was located at the positive maximum of PC1. The shapes of the remaining six tree species clustered in the middle of the morphospace between angiosperms and gymnosperms.

**Comparison between real tree photographs and illustrations**

The four real angiosperm tree species were visually well separated by multigroup discriminant analysis (CVA), mostly along the oak-like → poplar-like shape gradient (CV1; 88%) regarding crown shape and width (Fig. 6a). There is a significant difference between the shapes assigned to Populus and the shapes of the other three angiosperm species ($P < 0.0001$). The other three angiosperm tree shapes showed less 'interspecific' variation and rather similar group mean shapes (pairwise comparisons: Acer-Quercus: $P = 0.0001$, Fagus-Quercus: $P = 0.0025$, Fagus-Acer: $P = 0.0897$). The multigroup discriminant analysis (CVA) of the four real gymnosperm species also visually separated the species, but mostly along the pine-like → spruce-like shape gradient (CV1; 66%) concerning crown shape and trunk length (Fig. 6b). Pinus shapes were clearly separated from the other three gymnosperms ($P < 0.0001$ for all pairwise comparisons). While others showed slight overlap (Abies-Larix:$P = 0.0005$, Picea-Larix:$P = 0.0032$ and Picea-Abies:$P = 0.0917$). Adding the real tree illustrations to the real tree photographs did not significantly change the coherence of the four groups as described above (Fig. 6c,d). Pairwise comparisons of the four species revealed the same significant interspecific differences as in the previous analysis without the tree illustrations. Also in the combined analysis of real tree photographs and illustrations, the pairs Fagus-Acer and Picea-Abies showed no significant differences.

## Geometric-morphometric comparison of generated tree growth simulations and real tree photographs and illustrations (ground-truth data)

While PCA of the combined tree shape dataset (photographs + illustrations + simulations) showed overlap among the four species within the morphospace (Fig. 7a), CVA indicated significant separation of all four species (Fig. 7b), with ($P < 0.0001$) for all pairwise comparisons. The most important separating shape gradient puts more conical shapes (*Picea* and *Populus*-like) on one side and wider, less conical shapes on the other side of the first canonical axis (CV1; 57%). The second most important separating shape gradient distinguished angiosperm-like forms from gymnosperm-like forms (CV2; 25%).

Within the morphospace of each tree species, the respective generated tree growth simulations tended to occupy a distinct area, but did not show significant morphological distances to their real-world counterparts (Fig. 8). The four tree species exhibited different morphospace features in separate PCA ordinations, i.e, the main morphological trends (PC1+PC2) within the morphospace of *Quercus* (Fig. 8a) were different from those of the morphospace of Populus (Fig. 8b), *Picea* (Fig. 8c), and *Pinus* (Fig. 8d). In the case of *Quercus*, the generated simulations were well within the morphological trends given by the real tree shapes (Fig. 8a), i.e. they do not significantly exceed the range of both ordination axes. With Populus, the generated simulations largely exceeded the variation of the real tree shapes along the first ordination axis, but not along the second (Fig. 8b). The same was true for *Picea* (Fig. 8c). In the case of *Pinus*, the generated simulations only slightly exceeded the range of the first ordination axis and were well within the range of the second ordination axis (Fig. 8d).

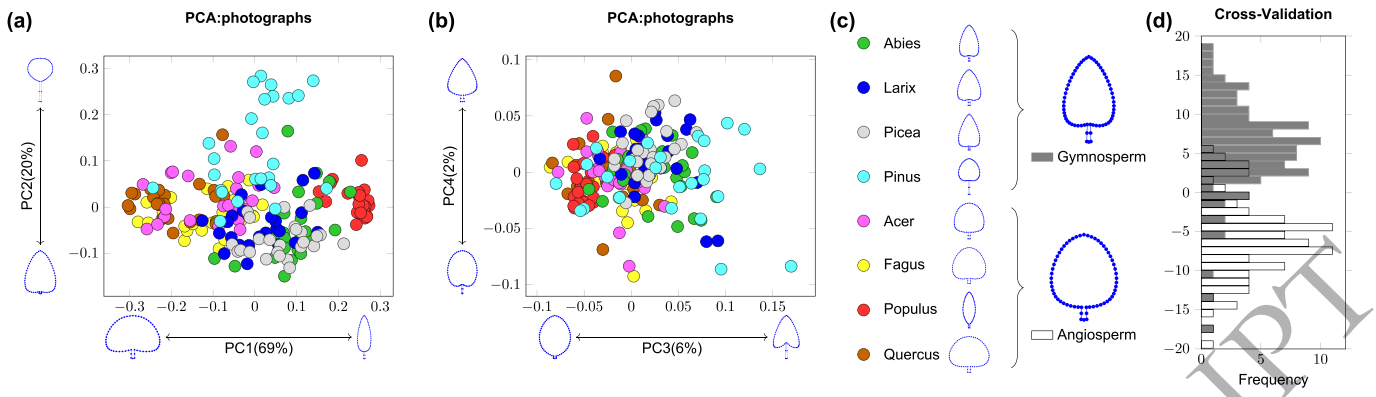


Fig. 5: Principal component analysis (PCA): a) Distribution of shapes of eight tree species (real tree photographs) along the first and second ordination axes, b) Distribution of shapes of eight tree species (real tree photographs) along the third and fourth ordination axes, c) Colors assigned to the eight tree species and the average shapes of the species, d) Two-group discriminant analysis of gymnosperm and angiosperm tree shapes; the plot shows cross-validation scores and average gymnosperm and angiosperm tree shapes. The wireframe plots next to the principal components (PC) in a) and b) represent shape changes associated with the ordination axes.

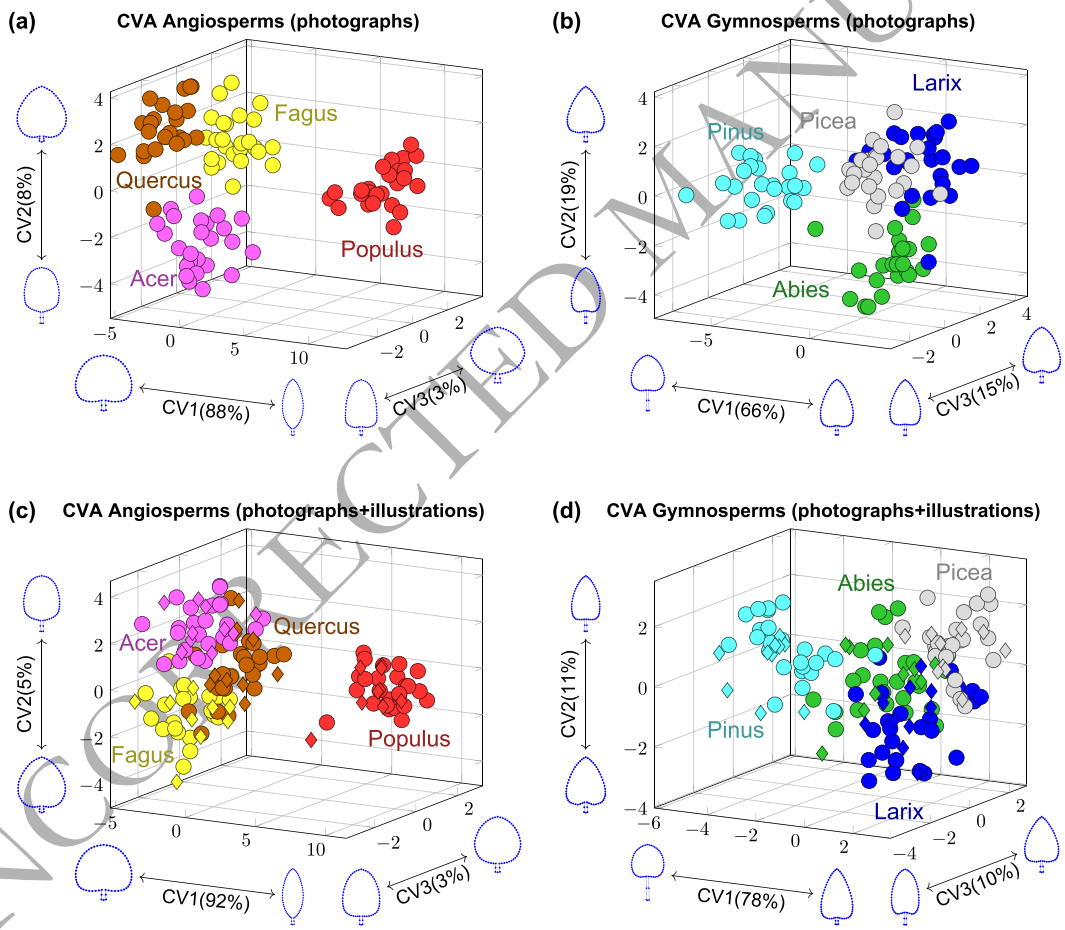


Fig. 6: Multigroup discriminant analysis (CVA): a) Shapes of four angiosperm tree species revealed from real tree photographs, b) Shapes of four gymnosperm tree species revealed from real tree photographs, c) Shapes of four angiosperm tree species revealed from real tree photographs (circle symbols) and illustrations (diamond symbols), d) Shapes of four gymnosperm tree species revealed from real tree photographs (square symbols) and illustrations (diamond symbols). The wireframe plots next to the canonical variates (CV) represent shape changes associated with the ordination axes.

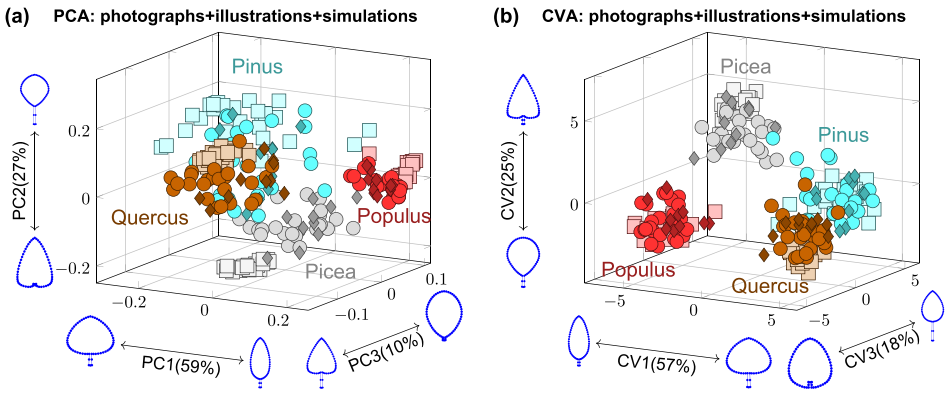


(c) Confusion matrix

| | Picea | Pinus | Populus | Quercus | accuracy |
|---|---|---|---|---|---|
| Picea | 183 | 1 | 0 | 2 | 0.9839 |
| Pinus | 3 | 176 | 1 | 6 | 0.9462 |
| Populus | 0 | 1 | 185 | 0 | 0.9946 |
| Quercus | 2 | 5 | 1 | 178 | 0.957 |
| precision | 0.9734 | 0.9617 | 0.9893 | 0.957 | |

Fig. 7: Principal component analysis (a) and multigroup discriminant analysis (b) of the shapes of two gymnosperm and two angiosperm tree species. c) displays the corresponding confusion matrix. Tree shapes were sampled from real tree photographs (circles), real tree illustrations (diamonds), and generated tree growth simulations (squares). The wireframe plots next to the principal components (PC) in a) and canonical variates (CV) in b) represent shape changes associated with the ordination axes.

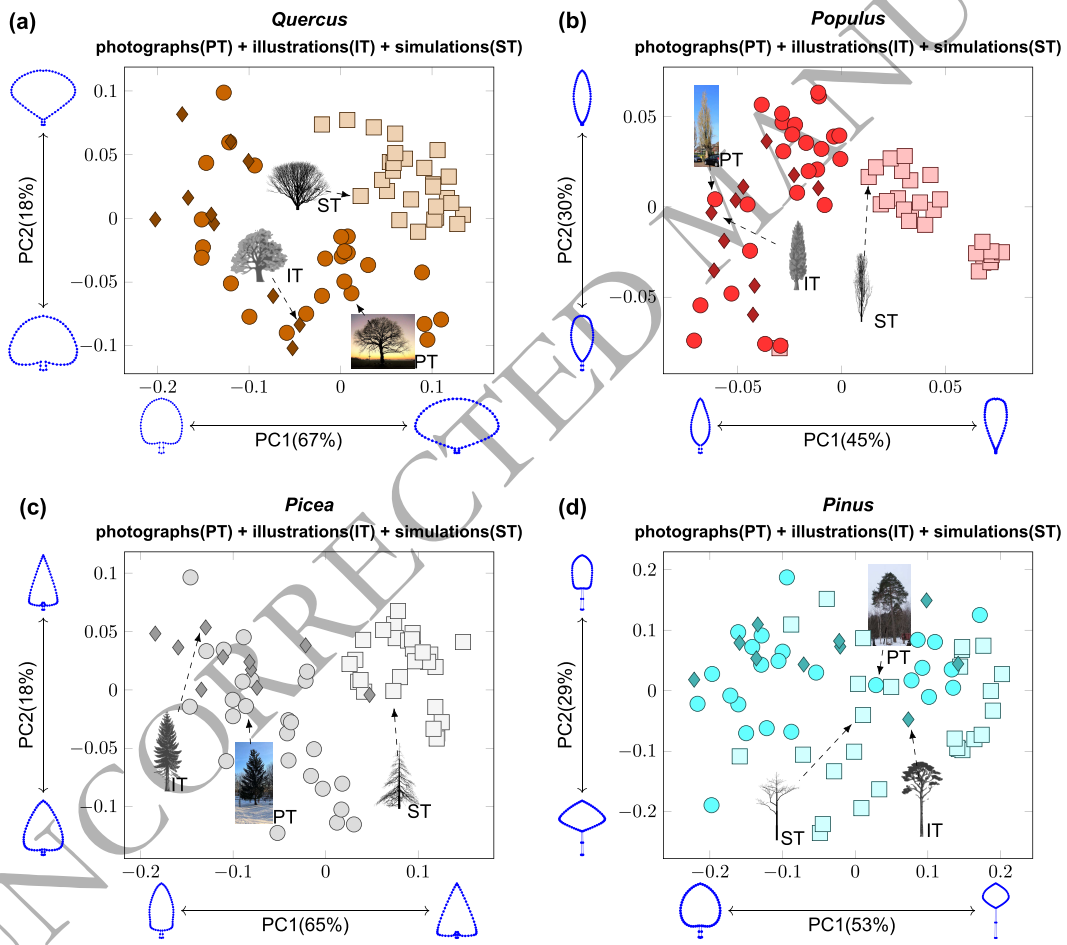


Fig. 8: Principal component analysis of the shapes of two angiosperm (a-b) and two gymnosperm (c-d) tree species. Tree shapes were sampled from real tree photographs (circles), real tree illustrations (diamonds), and generated tree growth simulations (squares). The wireframe plots next to the principal components (PC) represent shape changes associated with the ordination axes. Within each ordination plot, a characteristic real tree photograph, real tree illustration, and generated tree growth simulation are displayed.

## Discussion

Our FSPM approach contributes to the simulation of the growth of tree branching architectures based solely on the biological assumptions of plant growth logic. The simulated tree architectures, representing four different tree species (poplar, oak, spruce, pine), resulted from manual adjustment of 14 underlying biological parameters. It can be concluded that the parametrization of biological processes is validated as a reasonable way to simulate real growing trees. Phyllotaxis was represented by three parameters: number of leaves ($N$), divergence angle ($\varphi$), and branching angle ($\theta$). This allowed the creation of any natural leaf arrangement (Kadereit et al., 2014). The resulting leaf axils determine the produced buds and successfully represented lateral branches. This assumption works well for angiosperms, where each leaf has a bud. However, gymnosperms have hundreds of leaves per annual shoot, resulting in hundreds of small internodes and possible bud positions. Assuming that individual buds act as sinks for sugar and water, a distribution of buds along the branch is realistic. Therefore, we used the same spiral pattern to generate spruce, pine, poplar, and oak (Fig. 4). The vigor of each bud and its dormancy is controlled by the apical control of the internal flow. We have not considered effects such as positive xylem pressure (Schenk et al., 2021) and relate the water available per node to its water potential (Slatyer, 1960; Cabon et al., 2020). The customized biological parameter $\lambda$ (Palubicki et al., 2009) was used to approximate the water flow in the xylem. By combining the biological parameters for $\lambda$ and $\kappa$, we were able to reduce the mechanism of internal water flow and sugar storage. Changes in this resource allocation also determine the interaction with the environment. By controlling the internal water flow, we were also able to control the resource flow (Borchert and Honda, 1984) and branch density (Takenaka, 1994). But this was probably not enough to solve the complex growth mechanism of apical control. The term apical control encompasses several effects and the mechanisms behind them are poorly understood (Wilson, 2000; Hollender and Dardick, 2015). To simulate these effects, more dependencies on the internal phytohormone flux and its effect on the environment would be required. The simplified process resource transport is mainly based on water flow through sugar sinks. In addition, phytohormone transport should be considered. It may be distributed throughout the tree architecture by transport in the phloem. The assumed transport is subject to the source-to-sink concept (Fatichi et al., 2019), which could be implemented by the priority list concept (Palubicki et al., 2009). This would also determine the distribution of phytohormones and can control the flowering and fruiting activity of a branch. It would be possible to combine this source-to-sink concept with a complex photosynthesis calculation in a single model to simulate ecosystem gross primary production (Stocker et al., 2020). This would give more importance to external factors (humidity, temperature or vapor pressure deficit). However, such external parameters would likely have an additional effect on tree shape. Therefore, we assume that it would be necessary to keep the biological parameters for an FSPM as robust as possible (Louarn and Song, 2020).

The shape of a tree is a criterion for species identification (Duchemin et al., 2018). Our approach reduces the complexity of a complex 3D tree architecture to a silhouette-like 2D tree representation of both crown and stem, and used geometric morphometrics to compare real-world tree photographs, illustrations and our generated tree simulation counterparts. This approach was sufficient to distinguish different tree species (Fig. 7). The addition of the tree illustrations to the dataset did not alter the overall major morphometric trends already observed from the photographs. This resulted in a suitable dataset for evaluating simulated trees. Although the major segregating shape trends concerned crown shape, stem shape was also morphologically informative because of the significant relationship between crown radius and length and stem diameter (Franceschi et al., 2022). To the best of our knowledge, the evaluation of implemented biological tree growth assumptions as used in our study is completely novel. Geometric morphometrics revealed the following main differences between the four species: (a) poplar forms are narrow, spindle-shaped, and convex at the base of the crown, (b) spruce forms are also narrow and spindle-shaped, but concave at the base of the crown, (c) oak forms are broad and flat at the base of the crown, and (d) pine forms also tend to be broader, concave, and have long stems compared to poplar and spruce (Fig. 7b). Further improvements should concern the approach for comparing real and artificial tree architectures. A grown tree is influenced by several factors not considered in this study. For example, drought stress, tree age, light quality, and the daily path of the sun, which changes with geographic latitude, can all affect tree structure. In addition, the appearance of a reduced 2D tree shape representation is affected by camera settings, including perspective, distance, and field of view. Future attempts at more accurate tree shape comparisons should consider normalized 3D representations (Barbeito et al., 2017; Disney, 2019). In this study, we focused on the evaluation of solitary trees. Incorporating the effects of competition among multiple individuals will be a challenging task for future studies. In addition to evaluating the external shape of the tree, a further step will be to analyze the complex internal structure of the crown branching architecture. The complexity of this issue is mainly due to the immense intraspecific variation that affects any crown shape in nature (Pallardy, 2008; Caré et al., 2020).

Our FSPM-based approach yielded plausible visual simulations of realistic tree architectures, and the CVA (Fig. 7) showed significant separation of all species. The generated "species" clustered closer to their real-world counterparts and further far away from the other three tree types, i.e., the simulated spruce-like tree shapes clustered together with their real-world counterparts outside the clusters of pine, oak, and poplar (Fig. 7b). In contrast to previous work, we were able to quantify the effect of these parameters on the overall shape of the grown tree (Fig. 8; Fig. S4). The final shapes of the generated trees were mainly influenced by the photogravitropic set-point vector $P\vec{G}SV$ and the internal flow mechanism through the xylem flow ($\lambda$) and shedding rate ($\kappa$). With the used $P\vec{G}SV$, we successfully approximated the combination of graviceptive ($\beta$), photoceptive ($\nu$) and proprioceptive ($\gamma$) sensitivities to their basic assumptions (Honda et al., 1982; Greene, 1989; Bastien et al., 2013). However, we are also aware of the importance of the interplay of the above parameters with other parameters that have a less pronounced effect on shape. The simulations of the used FSPM could be partially distinguished from the ground truth in a pairwise comparison (Fig. 8). The used soft shadows of the light distribution model only approximate the complexity of the varying light quality and light sprectra across different layers. The model provides energy to the lower branches of the tree crown. This, combined with the even distribution of water, keeps the older branches alive. The generated tree of spruce, poplar and oak shows this effect with a short stem (Fig. 8a-c). Pinus with high values for shedding rate and xylem flow produced different stem shapes. This results in a better match between the generated

and ground truth data (Fig. 8d). The lower part of the simulated crowns are less bent to the ground. This can be attributed to the simplified tropism curvature and missing thigmomorphogenesis. For future use, $PG\vec{S}V$ should be improved to calculate the deflection under the weight of the branches using beam theory. This would be necessary to account for further factors such as wind (Pirk et al., 2014) or snow load. However, the exact calculation of the internal mechanisms has not been fully explored and requires further research (Moulia et al., 2022).

We presented an approach to apply geometric morphometrics to whole trees and showed that even a simple convexhull criterion provides enough information to distinguish tree species. The minimalist FSPM presented is based on the idea of a constant environment, without external damage and with a constant water supply. Only the internal processes of the plant control the distribution of resources. The limited set of parameters is based on simple approximations to real biological processes. Growth limitation occurs only due to lack of resources or lack of energy to convert them. Plausible visual results (tree shapes) were obtained and could be analysed with geometric morphometrics. This model will allow future studies to: (1) understand how crown shape and structure affect important ecological processes such as light interception, water and nutrient uptake, carbon assimilation, to assess their impact on overall tree growth and health, (2) predict tree growth and shape over time under different environmental conditions and management scenarios, (3) evaluate the effects of environmental factors and disturbances to understand the resilience, vulnerability and adaptation of trees to changing environments.

## Data and Materials Availability

The data that support the findings of this study are available online through the FigShare data repository (`DOI:10.6084/m9.figshare.23599083`).
(Data access during initial submission: `https://figshare.com/s/97bf96e8563347de1f08`)

## Conflict of Interest

The authors declare no conflict of interest.

## Funding

This study was funded by the German Ministry of Education and Research (BMBF) grant: 01IS20062, the German Federal Ministry for the Environment, Nature Conservation, Nuclear Safety and Consumer Protection (BMUV) grants: 3519685A08 and 3519685B08, 67KI2086 and the Thuringian Ministry for Environment, Energy and Nature Conservation grant: 0901-44-8652.

## Acknowledgements

We thank Dr. Kevin Karbstein for providing feedback on an earlier version of the manuscript. A special thank you goes to the curious plant observers at GBIF who provided the images analyzed in this study.

## Author contributions

TN and LH designed the research under guidance of JW and PM. TN contributed to data collection and performed the data analysis and visualisation with assistance from LH. TN has developed the tree simulation software and wrote the first draft of manuscript. All authors (TN, LH, JW, PM) contributed to revision and gave final approval for publication.

## References

J. Arvo and D. B. Kirk. Modeling plants with environment-sensitive automata. *Proceedings of Ausgraph '88*, pages 27–33, 1988. URL `https://api.semanticscholar.org/CorpusID:18525530`.

I. Barbeito, M. Dassot, D. Bayer, C. Collet, L. Drössler, M. Löf, M. Del Rio, R. Ruiz-Peinado, D. I. Forrester, A. Bravo-Oviedo, and H. Pretzsch. Terrestrial laser scanning reveals differences in crown structure of fagus sylvatica in mixed vs. pure european forests. *Forest Ecology and Management*, 405:381–390, 2017. ISSN 03781127. doi: 10.1016/j.foreco.2017.09.043. URL `https://www.researchgate.net/publication/320215483_Terrestrial_laser_scanning_reveals_differences_in_crown_structure_of_Fagus_sylvatica_in_mixed_vs_pure_European_forests`.

C. B. Barber, D. P. Dobkin, and H. Huhdanpaa. The quickhull algorithm for convex hulls. *ACM Transactions on Mathematical Software*, 22(4):469–483, 1996. ISSN 0098-3500. doi: 10.1145/235815.235821.

D. Barthélémy and Y. Caraglio. Plant architecture: A dynamic, multilevel and comprehensive approach to plant form, structure and ontogeny. *Annals of botany*, 99(3):375–407, 2007. ISSN 0305-7364. doi: 10.1093/aob/mcl260.

R. Bastien, T. Bohr, B. Moulia, and S. Douady. Unifying model of shoot gravitropism reveals proprioception as a central feature of posture control in plants. *Proceedings of the National Academy of Sciences*, 110(2):755–760, 2013. ISSN 1091-6490. doi: 10.1073/pnas.1214301109. URL `https://www.pnas.org/doi/10.1073/pnas.1214301109`.

R. Bastien, S. Douady, and B. Moulia. A unified model of shoot tropism in plants: Photo-, gravi- and propio-ception. *PLoS computational biology*, 11(2):e1004037, 2015. doi: 10.1371/journal.pcbi.1004037.

D. Boho, M. Rzanny, J. Wäldchen, F. Nitsche, A. Deggelmann, H. C. Wittich, M. Seeland, and P. Mäder. Flora capture: a citizen science application for collecting structured plant observations. *BMC Bioinformatics*, 21(1):576, 2020. ISSN 1471-2105. doi: 10.1186/s12859-020-03920-9. URL `https://bmcbioinformatics.biomedcentral.com/articles/10.1186/s12859-020-03920-9`.

F. L. Bookstein. Landmark methods for forms without landmarks: morphometrics of group differences in outline shape. *Medical Image Analysis*, 1(3):225–243, 1997. ISSN 1361-8415. doi: 10.1016/S1361-8415(97)85012-8. URL `https://www.sciencedirect.com/science/article/pii/S1361841597850128`.

R. Borchert and H. Honda. Control of development in the bifurcating branch system of tabebuia rosea: A computer simulation. *Botanical Gazette*, 145(2):184–195, 1984. ISSN 0006-8071. doi: 10.1086/337445.

G. F. Bueno, E. A. Costa, C. A. G. Finger, V. Liesenberg, and P. C. Da Bispo. Machine learning: Crown diameter predictive modeling for open-grown trees in the cerrado biome, brazil. *Forests*, 13(8):1295, 2022. ISSN 1999-4907. doi: 10.3390/f13081295. URL https://www.mdpi.com/1999-4907/13/8/1295.

A. Cabon, L. Fernández-de Uña, G. Gea-Izquierdo, F. C. Meinzer, D. R. Woodruff, J. Martínez-Vilalta, and M. de Cáceres. Water potential control of turgor-driven tracheid enlargement in scots pine at its xeric distribution edge. *New Phytologist*, 225(1):209–221, 2020. ISSN 1469-8137. doi: 10.1111/nph.16146. URL https://nph.onlinelibrary.wiley.com/doi/full/10.1111/nph.16146.

J. C. Caiza Guamba, D. Corredor, C. Galárraga, J. P. Herdoiza, M. Santillán, and M. C. Segovia-Salcedo. Geometry morphometrics of plant structures as a phenotypic tool to differentiate polylepis incana kunth. and polylepis racemosa ruiz & pav. reforested jointly in ecuador. *Neotropical Biodiversity*, 7(1):121–134, 2021. doi: 10.1080/23766808.2021.1906138.

O. Caré, O. Gailing, M. Müller, K. V. Krutovsky, and L. Leinemann. Crown morphology in norway spruce (picea abies [karst.] l.) as adaptation to mountainous environments is associated with single nucleotide polymorphisms (snps) in genes regulating seasonal growth rhythm. *Tree Genetics & Genomes*, 16(1), 2020. ISSN 1614-2942. doi: 10.1007/s11295-019-1394-x.

C. Coutand, B. Adam, S. Ploquin, and B. Moulia. A method for the quantification of phototropic and gravitropic sensitivities of plants combining an original experimental device with model-assisted phenotyping: Exploratory test of the method on three hardwood tree species. *PloS one*, 14(1):e0209973, 2019. doi: 10.1371/journal.pone.0209973.

M. Crimaldi, F. Cartenì, and F. Giannino. Vismaf: Synthetic tree for immersive virtual visualization in smart farming, part i: Scientific background review and model proposal. *Agronomy*, 11(12):2458, 2021. ISSN 2073-4395. doi: 10.3390/agronomy11122458. URL https://www.researchgate.net/publication/356751791_VISmaF_Synthetic_Tree_for_Immersive_Virtual_Visualization_in_Smart_Farming_Part_I_Scientific_Background_Review_and_Model_Proposal.

P. de Reffye, C. Edelin, J. Françon, M. Jaeger, and C. Puech. Plant models faithful to botanical structure and developmentr. In R. J. Beach, editor, *Proceedings of the 15th annual conference on Computer graphics and interactive techniques - SIGGRAPH '88*, pages 151–158, New York, New York, USA, 1988. ACM Press. ISBN 0897912756. doi: 10.1145/54852.378505.

J. Digby and R. D. Firn. The gravitropic set-point angle (gsa): The identification of an important developmentally controlled variable governing plant architecture. *Plant, cell & environment*, 18(12), 1995. ISSN 0140-7791. doi: 10.1111/j.1365-3040.1995.tb00205.x. URL https://pubmed.ncbi.nlm.nih.gov/11543210/.

M. Disney. Terrestrial lidar: a three-dimensional revolution in how we look at trees. *New Phytologist*, 222(4):1736–1741, 2019. ISSN 1469-8137. doi: 10.1111/nph.15517. URL https://nph.onlinelibrary.wiley.com/doi/10.1111/nph.15517.

F. K. Du, M. Qi, Y.-Y. Zhang, and R. J. Petit. Asymmetric character displacement in mixed oak stands. *New Phytologist*, 236(3):1212–1224, 2022. ISSN 1469-8137. doi: 10.1111/nph.18311. URL https://nph.onlinelibrary.wiley.com/doi/10.1111/nph.18311.

L. Duchemin, C. Eloy, E. Badel, and B. Moulia. Tree crowns grow into self-similar shapes controlled by gravity and light sensing. *Journal of the Royal Society, Interface*, 15(142), 2018. ISSN 1742-5662. doi: 10.1098/rsif.2017.0976. URL https://pubmed.ncbi.nlm.nih.gov/29743270/.

S. Fatichi, C. Pappas, J. Zscheischler, and S. Leuzinger. Modelling carbon sources and sinks in terrestrial vegetation. *New Phytologist*, 221(2):652–668, 2019. ISSN 1469-8137. doi: 10.1111/nph.15451. URL https://nph.onlinelibrary.wiley.com/doi/full/10.1111/nph.15451.

J. B. Fisher and H. Honda. Computer simulation of branching pattern and geometry in terminalia (combretaceae), a tropical tree. *Botanical Gazette*, 138(4):377–384, 1977. ISSN 0006-8071. doi: 10.1086/336937.

E. Franceschi, A. Moser-Reischl, M. A. Rahman, S. Pauleit, H. Pretzsch, and T. Rötzer. Crown shapes of urban trees-their dependences on tree species, tree age and local environment, and effects on ecosystem services. *Forests*, 13(5):748, 2022. ISSN 1999-4907. doi: 10.3390/f13050748. URL https://www.mdpi.com/1999-4907/13/5/748.

P. Galland, Y. Wallacher, H. Finger, M. Hannappel, S. Tröster, E. Bold, and F. Grolig. Tropisms in phycomyces: Sine law for gravitropism, exponential law for photogravitropic equilibrium. *Planta*, 214(6):931–938, 2002. ISSN 1432-2048. doi: 10.1007/s00425-001-0705-1.

GBIF. Gbif backbone taxonomy, 2022.

C. Godin and H. Sinoquet. Functional-structural plant modelling. *The New phytologist*, 166(3):705–708, 2005. doi: 10.1111/j.1469-8137.2005.01445.x. URL https://nph.onlinelibrary.wiley.com/doi/10.1111/j.1469-8137.2005.01445.x.

N. Greene. Voxel space automata: Modeling with stochastic growth processes in voxel space. In J. Lane, editor, *SIGGRAPH '89 conference proceedings*, Computer graphics, pages 175–184, New York, 1989. ACM Press. ISBN 0201504340. doi: 10.1145/74333.74351.

F. Hallé, R. A. A. Oldeman, and P. B. Tomlinson. *Tropical Trees and Forests: An Architectural Analysis*. Springer Berlin Heidelberg, Berlin, Heidelberg, 1978. ISBN 9783642811906.

C. A. Hollender and C. Dardick. Molecular basis of angiosperm tree architecture. *New Phytologist*, 206(2):541–556, 2015. ISSN 1469-8137. doi: 10.1111/nph.13204. URL https://nph.onlinelibrary.wiley.com/doi/full/10.1111/nph.13204.

H. Honda. Description of the form of trees by the parameters of the tree-like body: Effects of the branching angle and the branch length on the shape of the tree-like body. *Journal of Theoretical Biology*, 31(2):331–338, 1971. ISSN 00225193. doi: 10.1016/0022-5193(71)90191-3.

H. Honda, P. B. Tomlinson, and J. B. Fisher. Computer simulation of branch interaction and regulation by unequal flow rates in botanical trees. *American journal of botany*, 68(4):569–585, 1981. ISSN 0002-9122. doi: 10.1002/j.1537-2197.1981.tb07801.x.

H. Honda, P. B. Tomlinson, and J. B. Fisher. Two geometrical models of branching of botanical trees. *Annals of Botany*, 49(1):1–11, 1982. ISSN 0305-7364. doi: 10.1093/oxfordjournals.aob.a086218.

T. C. Hsiao and L.-K. Xu. Sensitivity of growth of roots versus leaves to water stress: Biophysical analysis and relation to water transport. *Journal of experimental botany*, 51(350):1595–1616, 2000. doi: 10.1093/jexbot/51.350.1595.

R. J. Jensen, K. M. Ciofani, and L. C. Miramontes. Lines, outlines, and landmarks: Morphometric analyses of leaves of acer rubrum, acer saccharinum (aceraceae) and their hybrid. *TAXON*, 51(3): 475, 2002. ISSN 0040-0262. doi: 10.2307/1554860.

J. W. Kadereit, C. Körner, B. Kost, and U. Sonnewald. *Strasburger – Lehrbuch der Pflanzenwissenschaften*. Springer Berlin Heidelberg, Berlin, Heidelberg, 2014. ISBN 978-3-642-54434-7. doi: 10.1007/978-3-642-54435-4.

C. P. Klingenberg. Morphoj: an integrated software package for geometric morphometrics. *Molecular Ecology Resources*, 11(2): 353–357, 2011. ISSN 1755-0998. doi: 10.1111/j.1755-0998.2010.02924.x. URL https://onlinelibrary.wiley.com/doi/full/10.1111/j.1755-0998.2010.02924.x.

W. Li, N. G. McDowell, H. Zhang, W. Wang, D. S. Mackay, R. Leff, P. Zhang, N. D. Ward, M. Norwood, S. Yabusaki, A. N. Myers-Pigg, S. C. Pennington, A. L. Pivovaroff, S. Waichler, C. Xu, B. Bond-Lamberty, and V. L. Bailey. The influence of increasing atmospheric co2 , temperature, and vapor pressure deficit on seawater-induced tree mortality. *New Phytologist*, 235(5):1767–1779, 2022. ISSN 1469-8137. doi: 10.1111/nph.18275. URL https://nph.onlinelibrary.wiley.com/doi/10.1111/nph.18275.

A. Lindenmayer and P. Prusinkiewicz. *Algorithmic Beauty of Plants*. The Virtual laboratory. Springer New York, New York, n edition, 1990. ISBN 1461384761.

Y. Liu, Y. Li, J. Song, R. Zhang, Y. Yan, Y. Wang, and F. K. Du. Geometric morphometric analyses of leaf shapes in two sympatric chinese oaks: Quercus dentata thunberg and quercus aliena blume (fagaceae). *Annals of Forest Science*, 75(4):1–12, 2018. ISSN 1297-966X. doi: 10.1007/s13595-018-0770-2. URL https://link.springer.com/article/10.1007/s13595-018-0770-2.

J. A. Lockhart. An analysis of irreversible plant cell elongation. *Journal of Theoretical Biology*, 8(2):264–275, 1965. ISSN 00225193. doi: 10.1016/0022-5193(65)90077-9. URL https://www.sciencedirect.com/science/article/pii/0022519365900779.

G. Louarn and Y. Song. Two decades of functional-structural plant modelling: now addressing fundamental questions in systems biology and predictive ecology. *Annals of botany*, 126(4):501–509, 2020. ISSN 0305-7364. doi: 10.1093/aob/mcaa143. URL https://www.ncbi.nlm.nih.gov/pmc/articles/PMC7489058/.

M. Makowski, T. Hädrich, J. Scheffczyk, D. L. Michels, S. Pirk, and W. Pałubicki. Synthetic silviculture. *ACM Transactions on Graphics*, 38(4):1–14, 2019. ISSN 07300301. doi: 10.1145/3306346.3323039.

R. Měch and P. Prusinkiewicz. Visual models of plants interacting with their environment. In J. Fujii, editor, *Proceedings of the 23rd annual conference on Computer graphics and interactive techniques*, pages 397–410, New York, NY, 1996. ACM. ISBN 0897917464. doi: 10.1145/237170.237279.

Y. Meroz. Plant tropisms as a window on plant computational processes. *New Phytologist*, 229(4):1911–1916, 2021. ISSN 1469-8137. doi: 10.1111/nph.17091. URL https://nph.onlinelibrary.wiley.com/doi/full/10.1111/nph.17091.

B. Moulia, E. Badel, R. Bastien, L. Duchemin, and C. Eloy. The shaping of plant axes and crowns through tropisms and elasticity: an example of morphogenetic plasticity beyond the shoot apical meristem. *New Phytologist*, 233(6):2354–2379, 2022. ISSN 1469-8137. doi: 10.1111/nph.17913. URL https://nph.onlinelibrary.wiley.com/doi/full/10.1111/nph.17913.

D. E. Moulton, H. Oliveri, and A. Goriely. Multiscale integration of environmental stimuli in plant tropism produces complex behaviors. *Proceedings of the National Academy of Sciences*, 117(51):32226–32237, 2020. ISSN 1091-6490. doi: 10.1073/pnas.2016025117.

H. C. Muller-Landau, K. C. Cushman, E. E. Arroyo, I. Martinez Cano, K. J. Anderson-Teixeira, and B. Backiel. Patterns and mechanisms of spatial variation in tropical forest productivity, woody residence time, and biomass. *New Phytologist*, 229(6):3065–3087, 2021. ISSN 1469-8137. doi: 10.1111/nph.17084. URL https://nph.onlinelibrary.wiley.com/doi/10.1111/nph.17084.

A. B. Nicotra, A. Leigh, C. K. Boyce, C. S. Jones, K. J. Niklas, D. L. Royer, and H. Tsukaya. The evolution and functional significance of leaf shape in the angiosperms. *Functional plant biology : FPB*, 38(7):535–552, 2011. ISSN 1445-4416. doi: 10.1071/FP11057. URL https://www.publish.csiro.au/fp/fp11057.

E. Nikinmaa, R. Sievänen, and T. Hölttä. Dynamics of leaf gas exchange, xylem and phloem transport, water potential and carbohydrate concentration in a realistic 3-d model tree crown. *Annals of botany*, 114(4):653–666, 2014. ISSN 0305-7364. doi: 10.1093/aob/mcu068. URL https://www.ncbi.nlm.nih.gov/pmc/articles/PMC4156122/.

S. G. Pallardy. *Physiology of Woody Plants*. Elsevier Science & Technology, Burlington, 3rd ed. edition, 2008. ISBN 9780080568713. URL https://ebookcentral.proquest.com/lib/kxp/detail.action?docID=343605.

W. Palubicki, K. Horel, S. Longay, A. Runions, B. Lane, R. Měch, and P. Prusinkiewicz. Self-organizing tree models for image synthesis. *ACM Transactions on Graphics*, 28(3):1, 2009. ISSN 07300301. doi: 10.1145/1531326.1531364.

G. Piovesan and F. Biondi. On tree longevity. *New Phytologist*, 231(4):1318–1337, 2021. ISSN 1469-8137. doi: 10.1111/nph.17148. URL https://nph.onlinelibrary.wiley.com/doi/10.1111/nph.17148.

S. Pirk, T. Niese, T. Hädrich, B. Benes, and O. Deussen. Windy trees. *ACM Transactions on Graphics*, 33(6):1–11, 2014. ISSN 07300301. doi: 10.1145/2661229.2661252.

T. Polasek, D. Hrusa, B. Benes, and M. Čadík. Ictree. *ACM Transactions on Graphics*, 40(6):1–15, 2021. ISSN 07300301. doi: 10.1145/3478513.3480519.

P. Prusinkiewicz, M. James, and R. Měch. Synthetic topiary. In D. Schweitzer, A. Glassner, and M. Keeler, editors, *Proceedings of the 21st annual conference on Computer graphics and interactive techniques - SIGGRAPH '94*, pages 351–358, New York, New York, USA, 1994. ACM Press. ISBN 0897916670. doi: 10.1145/192161.192254.

W. T. Reeves and R. Blau. Approximate and probabilistic algorithms for shading and rendering structured particle systems. *ACM SIGGRAPH Computer Graphics*, 19(3):313–322, 1985. ISSN 0097-8930. doi: 10.1145/325165.325250.

F. J. Rohlf. The tps series of software. *Hystrix, the Italian Journal of Mammalogy*, 26(1), 2015. ISSN 03941914. doi: 10.4404/hystrix-26.1-11264.

F. J. Rohlf and D. Slice. Extensions of the procrustes method for the optimal superimposition of landmarks. *Systematic Zoology*, 39(1):40, 1990. ISSN 00397989. doi: 10.2307/2992207. URL https://academic.oup.com/sysbio/article/39/1/40/1629843?login=true.

A. Runions, B. Lane, and P. Prusinkiewicz. Modeling trees with a space colonization algorithm. In E. Galin, editor, *Proceedings of the Third Eurographics conference on Natural Phenomena*, pages 63–70, Aire-la-Ville, Switzerland, 2007. Eurographics Association. ISBN 3-905673-29-0.

T. Sachs. Self-organization of tree form: A model for complex social systems. *Journal of Theoretical Biology*, 230(2), 2004. ISSN 00225193. doi: 10.1016/j.jtbi.2004.05.006. URL `https://pubmed.ncbi.nlm.nih.gov/15302551/`.

H. J. Schenk, S. Jansen, and T. Hölttä. Positive pressure in xylem and its role in hydraulic function. *New Phytologist*, 230(1):27–45, 2021. ISSN 1469-8137. doi: 10.1111/nph.17085. URL `https://nph.onlinelibrary.wiley.com/doi/full/10.1111/nph.17085`.

H. Schmidt. Schmidt–vogt, h., die fichte. ein handbuch in zwei bänden. i taxonomie, verbreitung, morphologie, ökologie, waldgesellschaften. xviii + 647 s., 304 abb., 60 übersichten. verlag paul parey, hamburg, berlin 1977. isbn 3–490–08216–8. preis: Leinen 198,— dm. *Feddes Repertorium*, 91(3):196–197, 1980. ISSN 0014-8962. doi: 10.1002/fedr.19800910311.

K. Shinozaki, K. Yoda, K. Hozumi, and T. Kira. A quantitative analysis of plant form – the pipe model theory. i. basic analyses. *Japanese Journal of Ecology*, 14 (3):97–105, 1964. doi: 10.18960/seitai.14.3{\textunderscore} 97. URL `https://www.jstage.jst.go.jp/article/seitai/14/3/14_KJ00001775191/_article/-char/ja/`.

R. O. Slatyer. Absorption of water by plants. *The Botanical Review*, 26(3):331–392, 1960. ISSN 1874-9372. doi: 10.1007/BF02860807. URL `https://link.springer.com/article/10.1007/BF02860807`.

B. D. Stocker, H. Wang, N. G. Smith, S. P. Harrison, T. F. Keenan, D. Sandoval, T. Davis, and I. C. Prentice. P-model v1.0: An optimality-based light use efficiency model for simulating ecosystem gross primary production. *Geoscientific Model Development*, 13(3):1545–1581, 2020. doi: 10.5194/gmd-13-1545-2020. URL `https://gmd.copernicus.org/articles/13/1545/2020/`.

A. Takenaka. A simulation model of tree architecture development based on growth response to local light environment. *Journal of Plant Research*, 107(3):321–330, 1994. ISSN 1618-0860. doi: 10.1007/BF02344260.

J. Vos, J. B. Evers, G. H. Buck-Sorlin, B. Andrieu, M. Chelle, and P. H. B. de Visser. Functional-structural plant modelling: a new versatile tool in crop science. *Journal of experimental botany*, 61(8):2101–2115, 2010. doi: 10.1093/jxb/erp345. URL `https://academic.oup.com/jxb/article/61/8/2101/485723?login=true`.

J. Weber and J. Penn. Creation and rendering of realistic trees. In S. G. Mair, editor, *Proceedings of the 22nd annual conference on Computer graphics and interactive techniques*, pages 119–128, New York, NY, 1995. ACM. ISBN 0897917014. doi: 10.1145/218380.218427.

B. F. Wilson. Apical control of branch growth and angle in woody plants. *American journal of botany*, 87(5):601–607, 2000. ISSN 0002-9122. URL `https://pubmed.ncbi.nlm.nih.gov/10811784/`.

M. Zelditch, D. Swiderski, and H. Sheets. *Geometric Morphometrics for Biologists*. Elsevier, 2004. ISBN 9780127784601. doi: 10.1016/B978-0-12-778460-1.X5000-5.

M. H. Zimmermann. Hydraulic architecture of some diffuse-porous trees. *Canadian Journal of Botany*, 1978. ISSN 1480-3305. doi: 10.1139/b78-274.

## List of Figures

Figure 7:

Principal component analysis (a) and multigroup discriminant analysis (b) of the shapes of two gymnosperm and two angiosperm tree species. c) displays the corresponding confusion matrix. Tree shapes were sampled from real tree photographs (circles), real tree illustrations (diamonds), and generated tree growth simulations (squares). The wireframe plots next to the principal components (PC) in a) and canonical variates (CV) in b) represent shape changes associated with the ordination axes.

Figure 8:

Principal component analysis of the shapes of two angiosperm (a-b) and two gymnosperm (c-d) tree species. Tree shapes were sampled from real tree photographs (circles), real tree illustrations (diamonds), and generated tree growth simulations (squares). The wireframe plots next to the principal components (PC) represent shape changes associated with the ordination axes. Within each ordination plot, a characteristic real tree photograph, real tree illustration, and generated tree growth simulation are displayed.